Topics in Catalysis 6 (1998) 87–99

Solid acid catalysts based on supported tungsten oxides

David G. Barton [a], Stuart L. Soled [b] and Enrique Iglesia [a,*]

[a] *Department of Chemical Engineering, University of California at Berkeley, Berkeley, CA 94720, USA*
E-mail: iglesia@cchem.berkeley.edu

[b] *Corporate Research Laboratory, Exxon Research and Engineering, Route 22 East, Annandale, NJ 08801, USA*

Supported WO_x clusters are active and stable catalysts for isomerization, dehydration, and cracking reactions. Brønsted acid sites form on WO_x clusters when a lower valent element replaces W^{6+} or when W^{6+} centers reduce slightly during catalytic reactions. WO_x clusters of intermediate size provide the balance between reducibility and accessibility required to maximize the number of surface H^+ species in WO_x–ZrO_2, zirconium tungstate, and oxygen-modified WC catalysts. H_2 is involved in the generation and maintenance of Brønsted acid sites during catalytic reactions on WO_x clusters.

Keywords: tungsten oxides, solid acids, acid-catalyzed reactions

1. Introduction

Many research groups continue to explore the catalytic properties of oxide-based strong solid acids in an attempt to eliminate environmental concerns caused by the use, regeneration, and disposal of liquid acids and halide-containing solids [1,2]. The challenge of obtaining acid site strength and density comparable to those in sulfuric acid, halides, or oxyhalides remains a formidable one; the smaller electronegativity differences in metal-oxygen bonds compared with metal-halide bonds limit the achievable acid strength. In oxide-based solid acids, protons balance net negative charges produced by the replacement of a high valent cation with one of lower valence or by the attachment of an anion to the surface of a neutral oxide support. In all cases, the net negative charge is balanced by protons. Among strong solid acids, sulfated and tungstated zirconia and supported heteropolyacids show interesting catalytic behavior and have attracted significant attention. Their mesoporous structures allow more facile transport of reactants and products than the restricted pore structures in microporous acids and minimize undesired side reactions favored by diffusional restrictions and long intrapellet residence times.

Effective solid acids require that metal cations or metal oxide clusters interact with oxide supports to form structures that stabilize the protons responsible for Brønsted acidity. These isolated metal-oxygen pairs or metal oxide clusters must resist sintering and decomposition during hydrocarbon reactions. The recent intense interest in sulfated zirconia appears to arise from the ability of zirconia to establish this environment for the sulfate ion. Yet, serious concerns remain about the long-term stability of zirconia-supported sulfate species in reducing and oxidizing environments that are typical of hydrocarbon reactions and of regeneration treatments [3].

Tungsten oxide species dispersed on zirconia supports (WO_x–ZrO_2) by impregnation with a solution of tungstate anions and subsequent oxidation treatments at high temperatures (873–1173 K) show strong acidity. Hino and Arata suggested, based on color changes of Hammett indicators ($H_0 \leqslant -14.52$), that acid sites stronger than 100% sulfuric acid may exist [4]; however, the use of this technique to measure acid strength of solids is often unreliable [5]. These authors also reported that WO_x–ZrO_2 catalyzes the isomerization of n-pentane at low temperatures, but found high selectivity to cracked products ($\sim$ 50%) even at low conversions [4]. Butene dimerization studies later confirmed that acid sites on WO_x–ZrO_2 give catalytic rates and selectivities comparable to those on SO_x–ZrO_2 for this reaction [6]. The addition of a metal component (e.g., $<$ 1 wt.% Pt) to WO_x–ZrO_2 and the presence of H_2 in the reactant mixture lead to active, stable, and selective catalysts for n-alkane isomerization reactions [7–12].

The structural richness of tungsten oxide species leads to several atomic arrangements that can exhibit the strong acidity required for reactions of alkanes at low temperatures. 12-Tungstophosphoric acid ($H_3PW_{12}O_{40}$) and WO_x–ZrO_2 appear to contain the strongest acid sites among tungsten oxide-based materials reported in the literature. The ability to delocalize a negative charge among several surface oxygen atoms in heteropolytungstate or isopolytungstate clusters allows hydrogen atoms in OH surface groups and hydrocarbons interacting with such OH groups to retain cationic character, if not as a stable species, at least during the formation of short-lived intermediates or activated complexes required in acid catalysis. In 12-tungstophosphoric acid, the negative charge of the PO_4^{3-} anion is shared throughout a neutral $(WO_3)_{12}$ shell and is balanced by protons accessible to reactants at the surface of this shell [13,14].

In WO_x–ZrO_2 catalysts, WO_x clusters of intermediate size delocalize a net negative charge caused by the slight reduction of W^{6+} centers in reactant environments containing H_2 or hydrocarbons [9]. This temporary charge

* To whom correspondence should be addressed.

imbalance leads to the formation of Brønsted acid $(WO_3)_m\{W^{6-n}O_3\}\{n\text{-}H^+\}$ centers on the zirconia support. These Brønsted acid sites on WO_x–ZrO_2 appear to form via a mechanism similar to that on heteropolytungstate clusters, but in this case, the charge imbalance is not permanent; it is reversible and created *in-situ* by the reducing environment of the acid-catalyzed reaction. WO_x–ZrO_2 catalysts have an advantage over heteropolytungstates in that they retain structural integrity during high temperature oxidative treatments (> 873 K), in contrast with heteropolytungstates that decompose to bulk WO_3 at much lower temperatures (~ 673 K).

In this review paper, we discuss several important examples of solid acids based on tungsten oxides with emphasis on the role of support and surface structures on the rate and selectivity of acid-catalyzed reactions. We also describe some recent unpublished results from our group with regard to the structure and isomerization pathways on WO_x–ZrO_2 and Pt/WO_x–ZrO_2 catalysts.

2. Early studies of acid catalysts based on tungsten oxides

Catalysts containing tungsten oxides have been used as solid acid catalysts since the turn of the century. They were the subject of an extensive review of their catalytic properties about thirty years ago [15]. In early studies, these materials were shown to be active catalysts for hydrocracking, dehydrogenation, isomerization, reforming, alcohol dehydration, and olefin oligomerization reactions. Bulk WO_3 was reported to be an active catalyst for several of these reactions, but high temperatures were required because of its low surface area and weak acid sites [15]. The density and strength of acid sites and the rate of catalytic reactions on tungsten oxide catalysts increase with slight reduction of the W^{6+} centers, which often occurs during catalytic reactions in reducing hydrocarbon environments. In addition, the more effective dispersion of WO_3 species on high surface area supports and the introduction of a heteroatom in order to create a permanent charge imbalance in the WO_3 structure increase the density and the strength of the acid sites.

Sabatier first reported that yellow WO_3 crystallites were readily reduced during alcohol reactions above 523 K to a stoichiometry corresponding to $WO_{2.5}$ [16]. This slightly reduced blue oxide was more active than WO_3 and was found to re-oxidize in air at room temperature [16]. Since this discovery, many studies have confirmed the enhanced catalytic activity of reduced bulk WO_3 for a variety of reactions. The reversible reduction-oxidation process and color change of bulk WO_3 is similar to that observed for hydrogen tungsten bronzes (H_xWO_3) prepared by exposing physical mixtures of Pt metal and bulk WO_3 to H_2 at room temperature [17]. H_2 dissociation on Pt metal sites leads to the slight reduction of WO_3 at room temperature by H-atom diffusion from Pt sites to WO_3 interstices.

At low temperatures, bulk WO_3 catalyzes metathesis reactions of alkenes via a mechanism that involves coordination of alkenes to W^{6+} Lewis centers [18]. Such pathways lead to reaction products that differ significantly from those formed in oligomerization-cracking reactions typical of Brønsted acid sites. The rate of propene metathesis reactions on WO_3 crystallites increases with increasing dispersion of these crystallites, which may be achieved by impregnation of aqueous solutions of ammonium paratungstate on high surface area supports (SiO_2, TiO_2, Al_2O_3, or ZrO_2) [18]. Highly dispersed WO_3 species (WO_x) with greater Brønsted acid site density can also be achieved by adding another metal oxide that forms mixed-oxide materials such as WO_3–P_2O_5, WO_3–MoO_3, $ZrW_{2\text{–}8}O_{0.5\text{–}3.5}$, or heteropolytungstates. The role of heteroatoms in intimate mixtures or as an oxide support can be two-fold: to increase the dispersion of WO_x clusters and to introduce a permanent charge imbalance that stabilizes protons and carbocationic species on the surface of these clusters.

3. Tungstated alumina catalysts (WO_x–Al_2O_3)

In 1937, Bliss and Dodge reported that dispersing WO_x species on Al_2O_3 enhanced the activity of bulk WO_3 catalysts for the hydration of ethylene [19]. More recent studies have addressed the structure of the WO_x species and its role in establishing the density and strength of acid sites for acid-catalyzed reactions of hydrocarbons [20–26].

WO_x species appear to interact strongly with sites on the surface of γ-Al_2O_3. These surface species inhibit the sintering of Al_2O_3 crystallites and the structural transformation of γ-Al_2O_3 into α-Al_2O_3 during high temperature oxidation treatments [20]. For example, a pure γ-Al_2O_3 sample shows a BET surface area of only 10 m^2/g after oxidation in air at 1323 K, but a sample containing 6 wt.% W has a surface area of 50 m^2/g. The resulting isolated species or small clusters of WO_x reduce in H_2 at much higher temperatures than bulk WO_3 or WO_x clusters supported on silica or zirconia.

WO_x surface coverage on Al_2O_3 supports increases with increasing temperature of oxidative pre-treatments which sinter the Al_2O_3 crystallites. Titration of the Brønsted acid sites with sterically hindered 2,6-dimethylpyridine shows that the Brønsted acid site density increases with increasing oxidation temperature (table 1) [24]. Lewis acid site density, measured by difference using 3,5-dimethylpyridine molecules that titrate both Lewis and Brønsted acid sites, decreases with increasing oxidation temperature (table 1) [24]. This increase in Brønsted acidity with increasing WO_x surface coverage appears to be related to the conversion of isolated tungstate groups into polytungstate clusters, which can delocalize protons among neighboring WO_x species. The appearance of polytungstate clusters as the oxidation temperature increases was detected in Raman spectra by the appearance of W–O–W bands with increasing WO_x coverage [22]. At WO_x coverages (> 3.2 W-

Table 1
Lutidine (2,6-dimethylpyridine and 3,5-dimethylpyridine) site titration results at 473 K from [24].

Catalyst	Oxidation temperature (K)	Brønsted acid sites[a] (μmol/m^2)	Lewis acid sites[b] (μmol/m^2)
γ-Al_2O_3	773	0	1.51
10% WO_3–Al_2O_3	773	0.14	1.36
10% WO_3–Al_2O_3	1223	0.38	1.13
Y-zeolite	773	1.8	0.47

[a] Number of Brønsted acid sites on WO_x–Al_2O_3 calculated from 2,6-dimethylpyridine uptake minus the uptake of Al_2O_3. [b] Number of Lewis acid sites calculated as the difference between 3,5-dimethylpyridine uptakes and number of Brønsted acid sites.

atoms/nm^2) where polytungstate clusters exist, W-L_I X-ray absorption near-edge spectra (XANES) resemble the spectrum of the distorted tungsten oxide octahedral symmetry in bulk WO_3 [23]. At low WO_x coverages (1.4 W-atoms/nm^2), the spectra resemble the spectrum of the tungsten oxide tetrahedral symmetry in $Al_2(WO_4)_3$, which suggests that isolated tetrahedral tungstate groups are responsible for the enhanced Lewis acidity at low WO_x coverage [23].

Highest gas-oil cracking rates were reported on WO_x–Al_2O_3 catalysts with surface coverages of about 2.4 W-atoms/nm^2 [24]. This surface density appears to lead to polytungstate clusters containing a sufficient number of W–O–W linkages for effective delocalization of the $H^{\delta+}$ species among neighboring close-packed WO_x species, but which retain a high density of surface WO_x groups required for a high acid site density [24]. The rate and selectivity for the isomerization of isobutane and 2-methyl-2-pentene and the thermal desorption spectra of NH_3 and lutidine probe molecules show that WO_x–Al_2O_3 catalysts contain moderately strong Brønsted acid sites, intermediate in strength between those on amorphous silica–alumina catalysts and on Y-zeolite [24,25]. WO_x–Al_2O_3 catalysts retain their activity for gas-oil cracking after high temperature hydrothermal treatments, whereas cracking rates on silica–alumina and zeolite catalysts decrease markedly after similar treatments (table 2) because of significant loss of surface area.

The introduction of a metal function (0.3 wt.% Pt) on WO_x–Al_2O_3 (8.4 wt.% W) leads to bifunctional alkane conversion reactions, in which metal sites catalyze alkane dehydrogenation and acid sites catalyze isomerization and β-scission reactions of alkenes [26]. Isomerization of 3,3-dimethylpentane at 623 K on these catalysts leads to a high ratio of (2,3) to (2,2) isomers among initial reaction products, consistent with isomerization that occurs predominately by methyl-shift rearrangements on acid sites and not by metal-catalyzed cyclic isomerization pathways [26]. Acid-catalyzed β-scission is the predominant reaction of n-heptane at 623 K (table 3). Slow hydride transfer reactions to surface intermediates lead to long surface residence times and a to high probability that they undergo β-scission reactions before they desorb as isomers.

Table 2
Effect of steaming on activity for East Texas Light gas-oil cracking [783 K, 303 kPa total, 283 kPa H_2O, $WHSV_{oil} = 1.4\ h^{-1}$] from [25].

Catalyst	Gas-oil cracking activity (cm^3 gas/g-cat·h)	
	Fresh catalyst	Catalyst steamed at 1144 K for 16 h
10% WO_3–Al_2O_3	0.45	0.41
Silica–alumina (Davison DA-1)	0.46	0.13
Zeolite (Davison FLX-5)	0.75	0.24

Table 3
n-Heptane isomerization product selectivity and rate on a Pt/WO_x–Al_2O_3 (0.3 wt.% Pt, 8.4 wt.% W) and oxygen-modified WC (O_2 chemisorbed at 800 K) catalysts [623 K, 4.4 kPa n-heptane, 96 kPa H_2] from [26].

	Pt/WO_x–Al_2O_3	WC/O-800 K
n-Heptane conversion (%)	13.4	12.9
Pt-Turnover rate (s^{-1})	0.55	0.17
Reaction selectivity (%)		
Hydrogenolysis	47.9	16.3
Isomerization	35.5	79.5
Cyclization	13.5	0.7
Dehydrogenation	3.1	3.5
Cracking pattern (%)		
1–2 (terminal)	15.7	32.8
2–3	22.0	30.4
3–4 (Mid-molecule)	62.4	36.8
Product selectivity (%)		
2-Methylhexane	14.9	37.3
3-Methylhexane	17.2	37.4
Ethylpentane	1.9	3.7
Dimethylpentanes	1.5	1.1
Alkylcyclopentanes	7.6	0.4
Toluene	5.9	0.3

4. Heteropolytungstates

Many studies have addressed the catalytic properties of heteropolytungstate clusters with Keggin structures, such as 12-tungstophosphoric acid ($H_3PW_{12}O_{40}$), and excellent review articles have described recent advances [13,14]. The $PW_{12}O_{40}^{3-}$ anion (i.e., the "conjugate base") contains the smallest negative charge among the different heteropolyanions with stable Keggin structures ($SiW_{12}O_{40}^{4-}$, $BW_{12}O_{40}^{5-}$, $GeW_{12}O_{40}^{4-}$, etc.). As a result, the corresponding acid form shows the strongest acidity and catalyzes reactions such as hydration of olefins, dehydration of alcohols, aromatic alkylation, conversion of methanol, oxygenation of alkenes, and

alcoholysis of epoxides [14]. 12-Tungstophosphoric acid consists of a central tetrahedral PO_4^{3-} anion encapsulated within a neutral $(WO_3)_{12}$ shell, on the surface of which three hydrogens with a net positive charge maintain the electroneutrality of the cluster. Thus, 12-tungstophosphoric acid can be thought of as an "encapsulated" form of phosphoric acid, which avoids the undesired properties of its liquid form. Similarly, the Si and B forms of heteropolytungstates become "encapsulated" forms of silicic and boric acids, which are much weaker than phosphoric acid in the liquid phase. Keggin structures corresponding to sequestered sulfuric acid ($H_2SW_{12}O_{40}$) are not available, apparently because the size and coordination symmetry of the central sulfur atom is inconsistent with a stable Keggin structure. If stable, $H_2SW_{12}O_{40}$ clusters with Keggin structures would provide stronger acid sites than currently available heteropolytungstate clusters.

The large and soft anionic clusters in Keggin structures provide the electron delocalization required for charge separation and for the formation of cationic complexes during acid-catalyzed reactions. Heteropolyacid salts, which are produced by partial exchange of the protons in the parent acid with alkali or other cations, form solid acids with morphological and solubility properties very different from those of the parent acid [27]. For example, partial exchange of 12-tungstophosphoric acid with Cs^+ ions converts the water-soluble low surface area (< 5 m^2/g) acid form into a water-insoluble precipitate. This porous solid reaches surface areas exceeding 100 m^2/g after about 80% of the H^+ species have been replaced by Cs^+ cations ($Cs_{2.5}H_{0.5}W_{12}O_{40}$). These acidic Cs salts were reported to be much more active per gram of catalyst than the H-form for alkylation of m-xylene and 1,3,5-trimethylbenzene with cyclohexene [28] and to contain slightly stronger acid sites as measured by a 2-methyl-2-pentene model reaction [29] (table 4). Other acid salts with large cations, such as Rb, K, and NH_4, also form small ($\sim$ 100 Å) water-insoluble precipitates with high surface areas and excellent catalytic properties, even though a large fraction of the hydrogens have been replaced by inactive alkali ions [13,27]. $H_3PW_{12}O_{40}$ contains a high density of protons located predominantly within dense crystallites that are accessible only to polar reactants, which tend to swell the structures and diffuse through the enlarged intracrystalline voids. These swollen structures of the acid forms of heteropolyoxoanions have been described as "pseudo-liquid" media by Misono and co-workers [30]. The insoluble acid salts appear to be superior catalysts because they contain a higher permanent surface area accessible to both polar and non-polar molecules and because their insoluble nature prevents the undesired dissolution and elution of soluble acid forms during catalytic reactions of polar molecules. This leaching of catalytic species causes long-term stability and environmental contamination problems.

Table 4
Catalytic activity for alkylation and acidity of the $H_3PW_{12}O_{40}$ and $Cs_{2.5}H_{0.5}PW_{12}O_{40}$ catalysts [28,29].

	$H_3PW_{12}O_{40}$	$Cs_{2.5}H_{0.5}PW_{12}O_{40}$
Surface area (m^2/g)	6	131
Acid amount (μmol/g)[a]	8–16	161
Acidity parameter (3MP2/4MP2)[b]	0.6	1.3
Activity (mmol/g-cat·h)[c]		
m-Xylene	1.4	24.7
Trimethylbenzene	26.2	1.4

[a] Measured by TPD of NH_3. [b] 2-Methyl-2-pentene isomerization selectivity ratio [523 K, 1 h]. [c] Initial rates of alkylation with cyclohexene [327 mmol x-xylene, 216 mmol 1,3,5-trimethylbenzene, 10 mmol cyclohexene, 373 K].

Impregnation of aqueous solutions of heteropolyacids on inert oxide supports can be used to attain the protonic form of the heteropolyacid Keggin structure with a small crystal size that increases the accessible external surface area [31–33]. In this manner, the full density of protons in the parent acid can be retained and sites can remain accessible to non-polar reactants that normally contact only the external protons in crystalline heteropolyacids. Supports that interact weakly with Keggin clusters (e.g., SiO_2) are preferred, because strongly interacting supports such as Al_2O_3 can lead to hydrolysis and decomposition of the clusters at low temperatures [29]. The limitations of these methods for supporting water-insoluble heteropolyacid salts have been recently overcome [29]. These new methods involve the synthesis of SiO_2 supported heteropolyacid Cs-salts by replacing silanol hydrogens (Si–OH) with Cs^+ (Si–OCs) at high pH and then impregnating the Cs_2O–SiO_2 sample with an aqueous solution of $H_3PW_{12}O_{40}$. The heteropolyacid precipitates as the acid salt upon contact with Cs^+ cations on the surface of SiO_2 to form highly dispersed anchored clusters with $Cs_{2.5}H_{0.5}PW_{12}O_{40}$ stoichiometry.

5. Oxygen-modified tungsten carbides

High surface area stoichiometric tungsten carbides (WC) can be prepared by direct carburization of WO_3 with CH_4/H_2 mixtures (1100 K), followed by a high temperature H_2 treatment (973 K, 0.8 h) to remove polymeric carbon that can block carbidic surface sites [34]. Alkane dehydrogenation and hydrogenolysis turnover rates on tungsten carbides are similar to those reported on supported noble metal catalysts [35]. Chemisorption of oxygen on WC surfaces inhibits the rate of these reactions and introduces Brønsted acid surface sites similar to those present in supported tungsten oxides [34,36]. Such acid sites catalyze hydroisomerization of alkanes only when tungsten carbide sites are also present.

These oxygen-modified tungsten carbides are bifunctional; they catalyze alkane dehydrogenation on WC sites and alkene rearrangements on WO_x surface species [26]. WO_x sites on the carbide surfaces also catalyze methanol dehydration and propylene oligomerization and cracking reactions [37], but they do not catalyze propylene metathesis reactions that occur on Lewis acid sites present on WO_x–Al_2O_3 and WO_x–SiO_2 catalysts. It appears that Lewis acid

sites provided by W^{6+} centers are converted into Brønsted acid sites on oxygen-modified WC by interactions of WO_x with spill-over hydrogen atoms formed by H_2 or C–H dissociation on WC sites [38].

Oxygen-modified tungsten carbides catalyze n-heptane isomerization with high selectivity ($> 70\%$) at 623 K (table 3) [26]. Kinetic and isotopic tracer data show that the reaction proceeds via sequential n-heptane dehydrogenation and heptene isomerization steps. At 623 K, n-heptane conversion rates are limited by rearrangements of intermediate heptenes on WO_x acid sites, but n-heptane dehydrogenation becomes increasingly rate-limiting as reaction temperature is increased. Isomer distributions on oxygen-modified WC are similar to those found on Pt/WO_x–Al_2O_3 and the initial isomers formed from 3,3-dimethylpentane reactions are consistent with methyl-shift isomerization pathways (table 3). The WC function catalyzes the rapid exchange of deuterium atoms into "unreacted" n-heptane and its reaction products at 623 K, suggesting that hydrogen adsorption-desorption steps are quasi-equilibrated during n-heptane reactions. The high selectivity towards cleavage of terminal C–C bonds indicates that smaller alkanes form in hydrogenolysis reactions on WC sites, rather than by the acid-catalyzed β-scission cracking pathways that account for the low isomerization selectivity on Pt/WO_x–Al_2O_3 catalysts. It appears that the more intimate contact between H_2 dissociation/alkane dehydrogenation sites and Brønsted acid sites in oxygen-modified WC samples leads to shorter carbocation residence times and to a lower probability of β-scission reactions than on Pt/WO_x–Al_2O_3. At lower reaction temperatures, thermodynamics favor the desired multibranched alkanes, but the lower equilibrium alkene concentrations make bifunctional pathways involving gas phase alkenes very slow. Stronger WO_x acid sites such as those on Pt/WO_x–ZrO_2 catalysts and a chain mechanism that avoids the requirement for gas phase olefin intermediates lead to significantly higher alkane hydroisomerization rates and selectivities at low temperatures. Pt/WO_x–ZrO_2 catalysts for n-heptane hydroisomerization reactions are described in detail in a later section of this review.

6. Zirconium tungstate catalysts

Zirconium tungstate solids are used as inorganic cation-exchangers, but their catalytic properties have not been widely studied. Ethylene hydration rates on amorphous zirconium tungstate ($ZrW_{2\text{–}8}O_{0.5\text{–}3.5}$) powders are similar on a volumetric basis to those reported on supported phosphoric acid catalysts used in commercial practice [39] (table 5). An active catalyst with a W/Zr ratio of 2.0 was prepared by mixing aqueous Na_2WO_4 and $ZrOCl_2$ solutions at room temperature to give a white gel-like precipitate, which was acidified using HCl before filtering. Filtered precipitates were oxidized at 723 K for 7 h to produce an amorphous pale-yellow solid with high surface area (100 m^2/g) [40]. These materials catalyze near equilibrium conversion of ethylene to ethanol at 553 K after an induction period. Apparently, the slow partial reduction of the W^{6+} centers, a process detected from stoichiometric conversion of ethanol to acetaldehyde during the induction period, leads to increased Brønsted acidity in these materials.

Table 5
Catalytic activity of HCl washed zirconium tungstate catalysts for vapor phase ethylene hydration [493 K, 101 kPa, $H_2O/C_2H_4 = 1.0$, SV = 2300 h^{-1}].

Catalyst	W/Zr (atom ratio)	Ethanol concentration (wt.%)
Zirconium tungstate	1.0	0.60
Zirconium tungstate	2.0	0.90
Zirconium tungstate	3.0	0.80
H_3PO_4/SiO_2		0.45

Procedures for the synthesis of zirconium tungstate are similar to those used in the synthesis of supported WO_x–ZrO_2 catalysts. Zirconium tungstates, however, contain significant amounts of residual chloride ions, very high WO_x concentrations, and they are typically oxidized at temperatures below ZrO_2 crystallization temperatures. The nature of the acid sites on zirconium tungstate has not been carefully examined, but it appears that it contains Brønsted acid sites similar to those on WO_x–ZrO_2. In both types of catalysts, active species consist of amorphous polytungstate species that become Brønsted acids only after *in-situ* partial reduction during catalytic reactions. The residual electron-withdrawing chloride ions in zirconium tungstate powders, may increase the acid strength, but can cause corrosion and contamination problems by eluting as HCl during catalytic reactions.

7. Isopolytungstate clusters suported on zirconia (WO_x–ZrO_2)

WO_x–ZrO_2 powders were first reported to contain strong acid sites by Hino and Arata [4]. They reported low temperature n-butane and n-pentane isomerization activity on WO_x–ZrO_2 catalysts prepared by impregnating $ZrO_x(OH)_{4-2x}$ with aqueous ammonium metatungstate (13 wt.% W) and subsequent high temperature oxidation (1073 K). n-Pentane isomerization rates decreased markedly when metatungstate solutions were impregnated on crystalline ZrO_2 supports instead of amorphous $ZrO_x(OH)_{4-2x}$ supports, suggesting that hydrated WO_x species combine with $ZrO_x(OH)_{4-2x}$ surface sites and that such sites are not available after crystalline tetragonal or monoclinic ZrO_2 structures are formed. It appears that the initial formation of dispersed tungstate species occurs via anion exchange or condensation reactions of hydrated aqueous tungstate anions with surface OH species in $ZrO_x(OH)_{4-2x}$. The resulting high dispersion of WO_x species inhibits the crystallization and sintering of the ZrO_2 support crystallites and provides a material that can be sintered in a controlled manner during subsequent oxidation treatments. The sintering of the ZrO_2 support crystallites leads to the formation of WO_x clusters of varying size and catalytic properties.

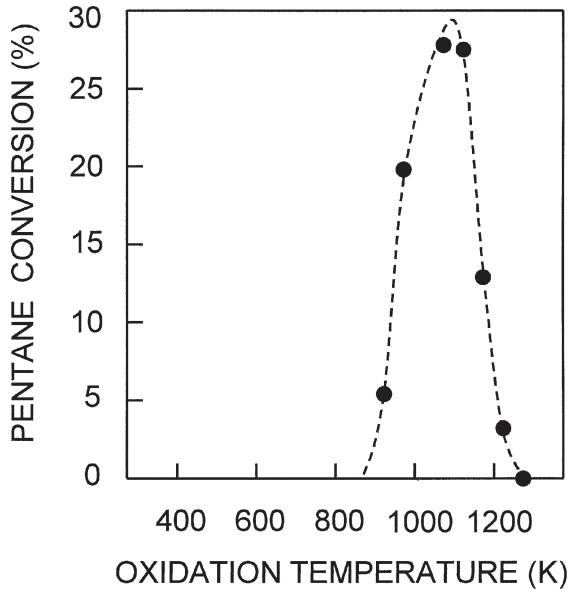

Figure 1. The effects of oxidation temperature on n-pentane isomerization [0.5 g catalyst, 13 wt.% W, 553 K, helium 10 cm^3/min, 1 μl n-C_5 pulse] (adopted from [4]).

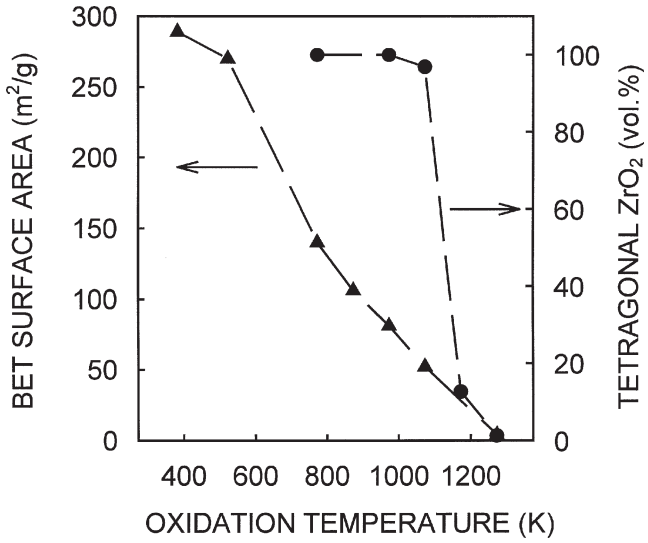

Figure 2. The effects of oxidation temperature on BET surface area and crystal modification of the zirconia support (7.9 wt.% W) [12].

n-Pentane isomerization rates depend strongly on the temperature at which impregnated samples are treated in air (figure 1) [4]. High isomerization rates occur in a narrow range of high oxidation temperatures (900–1250 K), during which loss of surface occurs and WO_x surface density increases. When n-pentane isomerization reactions are carried out in helium on these catalysts, selectivity to cracking products is high ($\sim$ 50%) and the catalysts deactivate rapidly.

The addition of small concentrations of a metal component ($<$ 0.5 wt.% Pt) to WO_x–ZrO_2 catalysts and the presence of H_2 in the reactant stream lead to very active, selective, and stable catalysts for n-alkane hydroisomerization at 473 K [8,9,12]. The metal function increases the rate of hydrogen transfer to isomerized intermediates, causing their desorption as isoalkanes before undesired β-scission reactions occur. In addition, metal sites appear to be involved in the formation of Brønsted acid sites via spillover of hydrogen adatoms from metal sites to WO_x species during the initial stages of the reaction. In the absence of H_2 and H–H dissociation sites, isomerization still occurs but via the sacrificial use of reactants to form surface hydrogen species. The desorption of the H species as H_2 during hydrocarbon reactions, however, leaves unsaturated hydrocarbon fragments permanently attached to the surface and leads to fast deactivation and to a limited number of catalytic turnovers.

In our studies, WO_x–ZrO_2 samples were prepared using previously reported synthesis methods [4], but over a wider range of composition and oxidation temperatures. High surface area $ZrO_x(OH)_{4-2x}$ was prepared via hydrolysis of $ZrOCl_2$ solution using slow addition of NH_4OH to raise the pH to a value of 10. After removing residual chloride ions by washing, the precipitate was dried and impregnated to incipient wetness with a solution of ammonium metatungstate ($(NH_4)_6H_2W_{12}O_{40}$) and then oxidized at high temperatures (873–1100 K) in dry air. Pt (0.3 wt.%) was introduced into some of the oxidized WO_x–ZrO_2 samples by incipient wetness with a solution of tetraammine platinum hydroxide, followed by decomposition in air at 723 K, and reduction in H_2 at 523 K.

BET surface area and X-ray diffraction measurements show that WO_x surface species inhibit zirconia sintering and its tetragonal to monoclinic phase transformation during the oxidative treatments required for the synthesis of active catalysts. $ZrO_x(OH)_{4-2x}$ powders show high surface areas (289 m^2/g) after drying at 383 K. At 1073 K, a typical oxidation temperature leading to WO_x–ZrO_2 samples with high activity, pure ZrO_2 has a very low surface area (4 m^2/g) and consists of large monoclinic crystals. Impregnation with near monolayer WO_x surface coverages (6 W-atoms/nm^2) results in higher surface areas (51 m^2/g) and small tetragonal ZrO_2 crystallites after oxidation at 1073 K. Three-dimensional growth of bulk WO_3-like species becomes detectable by X-ray diffraction and UV-visible measurements as this saturation coverage is exceeded. Tungsten surface densities above 10 W-atoms/nm^2 lead to lines corresponding to bulk WO_3 in X-ray diffraction patterns.

The structure and size of ZrO_2 crystallites can be controlled by adjusting the oxidation temperature and the W concentration. At a given W concentration (e.g., 7.9 wt.% W), the BET surface area and the tetragonal content in ZrO_2 decrease markedly with increasing oxidation temperature (figure 2). WO_x species inhibit the sintering and the transformation to monoclinic ZrO_2 crystallites, but as the oxidation temperature increases tetragonal ZrO_2 crystallites ultimately agglomerate and transform into monoclinic crystallites when a critical crystallite diameter is reached [41]. At a given oxidation temperature (e.g., 1073 K), surface area and tetragonal content increase with increasing W-loading up to 7.9 wt.% W (figure 3)

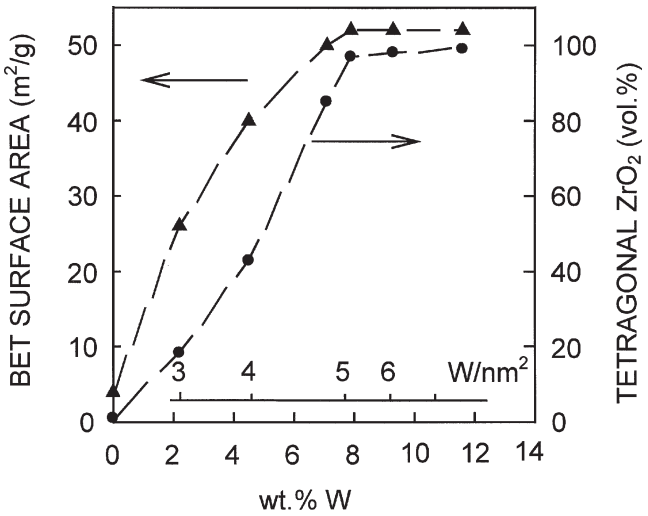

Figure 3. The effects of W loading on BET surface area and crystal modification on the zirconia support (1073 K oxidation) [12].

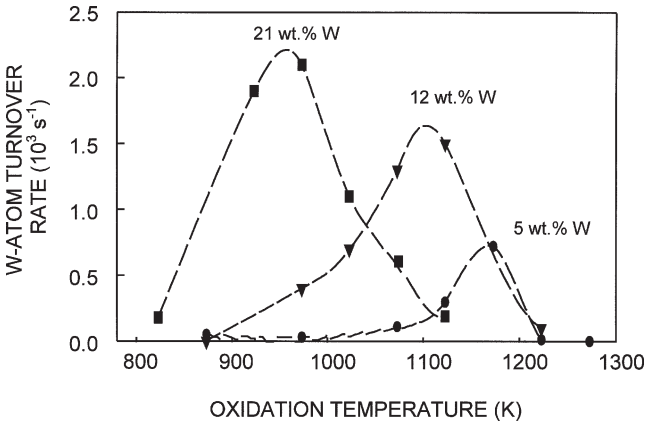

Figure 4. Initial o-xylene isomerization turnover rates at several oxidation temperatures and W-loadings in gradientless glass recirculating batch reactor [523 K, 104 kPa H_2, 0.66 kPa o-xylene] [12].

and then remain constant. It appears that $ZrO_x(OH)_{4-2x}$ powders contain an intrinsic number of strong binding sites for metatungstate ions ($\sim$ 8 wt.% W), which must be occupied in order to inhibit locally crystallite growth and re-crystallization into the thermodynamically stable monoclinic phase [12]. Impregnation with metatungstate ions beyond this required surface coverage leads to weakly held tungstate groups, which agglomerate into WO_x clusters and bulk WO_3 crystallites without additional stabilization of the ZrO_2 support.

Control of the W concentration and of the temperature of oxidation treatments can be used in order to design catalysts with a specific WO_x surface density and a high surface area. For example, WO_x–ZrO_2 samples containing similar WO_x surface densities, but very different total surface areas, were prepared by impregnation and controlled synthesis procedures. A sample with 22 wt.% W oxidized at 823 K had a total surface area of 140 m^2/g, but the same surface density (5.0 W-atoms/nm^2) as a 7.9 wt.% W sample oxidized at 1073 K and exhibiting a much lower surface area (51 m^2/g).

Acid-catalyzed skeletal isomerization of o-xylene to m- and p-xylene (523 K, 0.67 kPa o-xylene, 106 kPa H_2) was used in our study in order to examine the acid properties of WO_x–ZrO_2 catalysts. Xylene isomerization reactions proceed on Brønsted acid sites via protonation-deprotonation of xylenes with intervening intramolecular methyl shifts that form meta and para isomers before desorption. The selectivity to disproportionation products (toluene and trimethylbenzenes) was very low ($< 5\%$), suggesting that bimolecular isomerization pathways [42] are not involved in xylene isomerization reactions on WO_x–ZrO_2 catalysts at our reaction conditions. WO_x–ZrO_2 samples with varying W-loadings (2–21 wt.% W) and treated at several oxidation temperatures (823–1100 K) were examined using o-xylene isomerization reactions.

o-Xylene isomerization turnover rates (per W-atom) pass through a maximum value (0.0017 s^{-1}) at intermediate W concentrations (12 wt.% W) for samples treated in air at 1073 K. At each W-loading (5, 12 or 21 wt.% W), isomerization turnover rates also pass through a maximum value as the oxidation temperature increases (figure 4). The oxidation temperature at which this maximum value occurs decreases with increasing W-loading. These data suggest that an intermediate WO_x surface density may be required for high densities of Brønsted acid sites. When o-xylene isomerization turnover rates are plotted as a function of WO_x surface density for all WO_x–ZrO_2 catalysts tested, they merge into a single curve with a sharp maximum at about 10 W-atoms/nm^2 (figure 5). This WO_x surface density represents about twice the theoretical monolayer coverage of WO_x octahedra on a ZrO_2 surface. The narrow range of WO_x surface densities over which WO_x–ZrO_2 samples become active catalysts suggests that high isomerization turnover rates require the presence of WO_x clusters within a narrow range of cluster size, which appear to form selectively as a coverage of 10 W-atoms/nm^2 is reached. These clusters appear to be large enough to delocalize a net negative charge caused by the slight reduction of W^{6+} with H_2 leading to the formation of $W^{6-n}O_3(n\text{-}H^+)$ centers on the zirconia surface, but small enough to contain the resulting protons predominantly at crystallite surfaces rather than at inaccessible intracrystallite positions.

The requirement for slight reduction of W^{6+} centers in WO_x clusters of intermediate size is consistent with the strong effect of H_2 on the rate of o-xylene isomerization on WO_x–ZrO_2 catalysts. The addition of dihydrogen (101 kPa) increases steady-state o-xylene isomerization rates by more than a factor of four on WO_x–ZrO_2 at 523 K, suggesting the activation and involvement of H_2 during "monofunctional" acid-catalyzed reactions on WO_x–ZrO_2 [12]. The absence of H_2 leads to the irreversible loss of active sites, apparently as the result of H_2 desorption and the concomitant destruction of Brønsted acid sites, formed initially by the sacrificial use of hydrogen atoms from reactants during o-xylene reactions. Desorption of such H-atoms causes the adsorption of the unsaturated coproduct of the initial activation reaction to become irre-

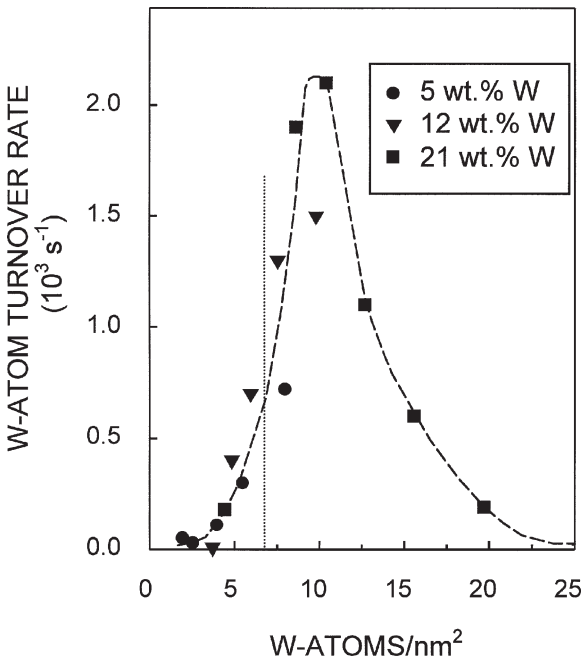

Figure 5. The influence of WO_x surface density on *o*-xylene isomerization turnover rates [523 K, 104 kPa H_2, 0.66 kPa *o*-xylene] [12]. The vertical dotted line marks the theoretical monolayer capacity of tetragonal ZrO_2.

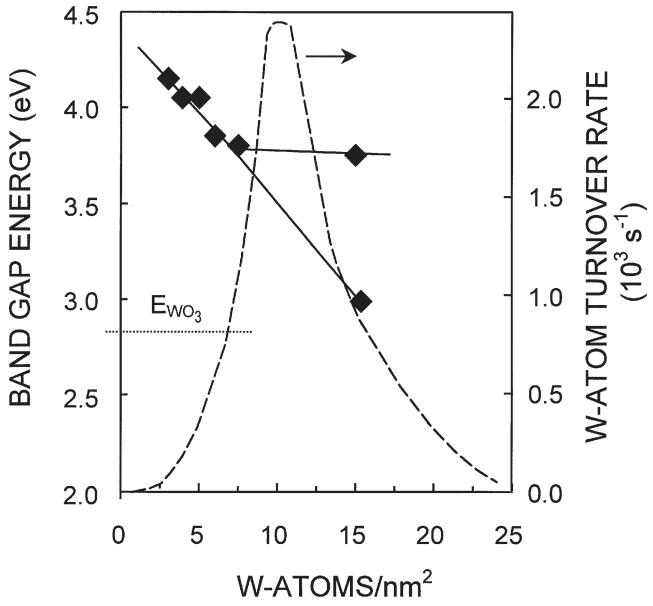

Figure 6. Direct band gap energy from UV-visible spectra of WO_x–ZrO_2 catalysts (1073 oxidation) overlaid on *o*-xylene isomerization rate data from figure 4 (adopted from [9]).

versible. Slow exchange of deuterium during reactions of *o*-xylene/D_2 mixtures shows that H_2 does not participate in hydrogen transfer elementary steps during xylene isomerization, but it is instead involved in the infrequent regeneration of acid sites lost in hydrogen desorption side reactions during *o*-xylene isomerization [12]. These Brønsted acid sites consist of $W^{6-n}O_3(n\text{-}H^+)$ centers, which are formed either by hydrogen migration from H–H or C–H dissociation sites to neutral WO_x clusters.

Previously reported electronic spectra in the UV-visible energy range for WO_x–ZrO_2 samples and other WO_x-containing samples [9] are consistent with the growth of WO_x clusters as the WO_x surface density increases. All WO_x–ZrO_2 samples show a maximum absorbance near 4.8–4.9 eV, which corresponds to ligand-to-metal charge transfer transitions. UV-visible spectra show that isolated WO_x species are not present in any WO_x–ZrO_2 sample after 1073 K oxidation and that all samples contain significant concentrations of polymeric –W–O–W– groups. A second band that appears at low energies (2.9 eV) in the spectra of samples with high WO_x surface densities ($>$ 10 W-atoms/nm^2) shows that WO_3 crystallites with different electronic properties can co-exist with amorphous WO_x clusters [9].

The low-energy absorption edge in UV-visible electronic spectra is sensitive to cluster size in the 1–10 nm range for many semiconductors, including WO_3 [43]. In this size range, the large fraction of atoms residing at the surface alters the cluster electronic properties. As a result, the energy gap between the valence and conduction bands increases with decreasing cluster size. This energy gap ranges from 2.8 eV for crystalline bulk WO_3 to 6.22 eV for the HOMO-LUMO gap in isolated WO_4^{2-} (aq.) ions. Optical absorption edge energies for WO_x–ZrO_2 samples oxidized at 1073 K were obtained from UV-visible spectra using procedures based on direct transitions between valence and conduction bands [44]. Direct band gap energies decrease monotonically from 4.15 to 3.80 eV as the WO_x surface density increases from 3.1 to 7.5 W-atoms/nm^2 and then become constant at higher surface densities ($>$ 7.5 W-atoms/nm^2) (figure 6) [9]. This monotonic decrease in the band gap energy suggests that average WO_x cluster size increases with increasing WO_x surface density in a range where marked increases in *o*-xylene isomerization rates also occur. The spectra of samples with high WO_x surface densities ($>$ 10 W-atoms/nm^2), however, show two distinct direct band gaps (absorption edges). The low-energy absorption edge reflects the presence of WO_3 crystallites with bulk-like electronic properties, which co-exist with WO_x clusters of intermediate size. The high-energy absorption edge position remains constant (3.8 eV) for all WO_x–ZrO_2 catalysts within the range of WO_x surface densities leading to high *o*-xylene isomerization turnover rates (6–15 W-atoms/nm^2) (figure 6). Thus, UV-visible spectra suggest that WO_x clusters with intermediate size, defined as those with absorption edges similar to ammonium metatungstate (3.5 eV), lead to WO_x–ZrO_2 samples with maximum activity.

X-ray absorption near edge spectroscopy at the W-L_I edge (12100 eV) is sensitive to the local coordination and symmetry of the W-atom absorbers. The pre-edge feature at -5 eV reflects a 2s $\rightarrow$ 5d electronic transition that is not allowed in octahedral (centrosymmetric) structures, but which occurs in tetrahedral or distorted octahedral structures because of d–p orbital mixing [45]. Previously, this pre-edge feature was used to detect the presence of 4- and

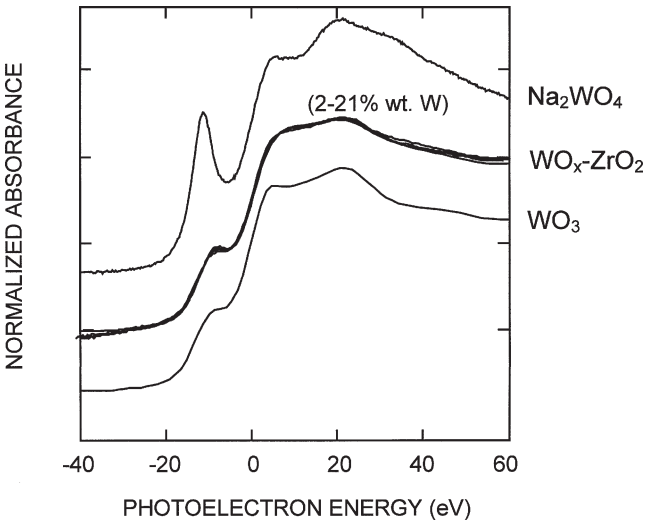

Figure 7. W-L_I X-ray absorption near-edge spectra after dehydration (He, 673 K) for WO_x–ZrO_2 (2–21 wt.% W) and Na_2WO_4 and WO_3 reference materials.

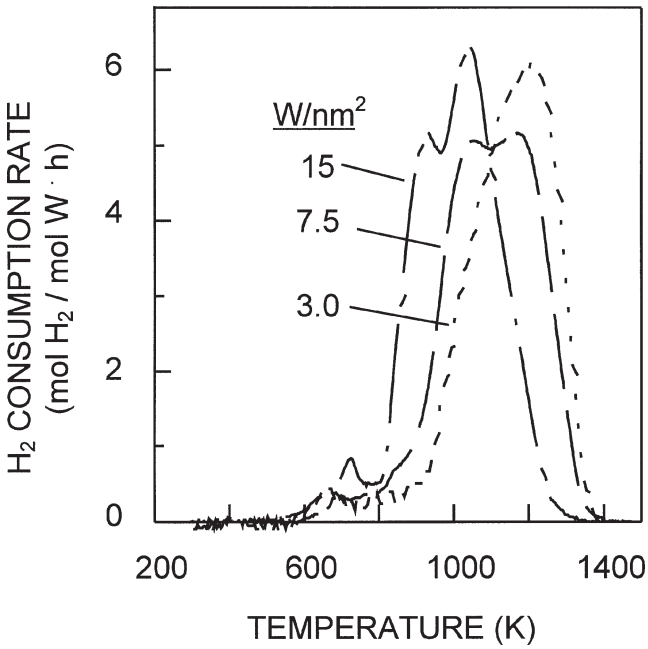

Figure 8. The influence of WO_x surface density on the temperature programmed reduction profiles of WO_x–ZrO_2 samples [10 K/min, 80 cm^3/min of 20% H_2/Ar mixture, 0.08–0.02 g] [9].

6-coordinated W atoms on WO_x–Al_2O_3 [23]. The degree of W coordination on Al_2O_3 supports increases with increasing concentration of WO_x species and with the extent of hydration of the catalyst samples [23].

Our studies show that W atoms in WO_x–ZrO_2 samples reside in distorted octahedral environments similar to those present in bulk WO_3 at all WO_x concentration and pretreatment conditions. Figure 7 shows the W-L_I absorption edges after dehydration (in He at 673 K) for several WO_x–ZrO_2 samples with different W concentrations oxidized at 1073 K (2–21 wt.% W) and for two standards: Na_2WO_4 (tetrahedral) and WO_3 (distorted octahedral) bulk powders. All WO_x–ZrO_2 samples show strikingly similar near-edge X-ray absorption spectra. Clearly, none of the WO_x–ZrO_2 samples have W-atoms in the tetrahedral symmetry of the Na_2WO_4 standard, but instead have W-atoms with distorted octahedral environments, similar to those found in bulk WO_3 crystallites.

Temperature-programmed reduction of supported metal oxides in hydrogen is also sensitive to the cluster size and coverage of surface oxides [46]. For example, isolated WO_x species on Al_2O_3 reduce at much higher temperatures than bulk WO_3 crystallites [21]. Reduction peaks for WO_x–ZrO_2 samples are very broad (600 K) and reduction occurs at much lower temperatures than for WO_x–Al_2O_3 samples at similar WO_x surface densities. The reduction of WO_x clusters of intermediate size on ZrO_2 occurs at temperatures typical of those required for the reduction of heteropolytungstate clusters (figure 8) [47]. Whereas, the reduction of WO_x species at low WO_x coverage is strongly influenced by the ZrO_2 support and occurs at higher temperatures than bulk WO_3. The larger WO_x clusters present at higher WO_x surface densities delocalize the initial net negative charge caused by reduction and lead to species that reduce at lower temperatures; these species then act as H_2 dissociation centers that increase the rate of subsequent reduction steps. The ability to delocalize the net negative charge on the conjugate base may be linked to both the strong acidity that appears near saturation WO_x coverage on ZrO_2 and to the easier initial reduction of WO_x clusters as surface coverage and cluster size increase. It appears that a critical cluster size is required for both reduction and Brønsted acidity, because the appearance of the latter may require the incipient reduction of neutral WO_3 clusters by H-atoms.

The addition of a metal function (0.3 wt.% Pt) to WO_x–ZrO_2 leads to the selective hydroisomerization of C_7^+ alkanes at 373–473 K, without the extensive cracking observed on Pt/SO_x–ZrO_2 and on zeolites promoted by metals [8,9,48]. At 473 K, n-heptane isomerization turnover rates are similar on Pt/WO_x–ZrO_2 and Pt/SO_x–ZrO_2 (based on W and S-atoms, respectively), but Pt/WO_x–ZrO_2 is significantly more selective to heptane isomers (85% at 50% n-heptane conversion). At higher reaction temperatures, Pt/WO_x–ZrO_2 catalysts are significantly more active than Pt/SO_x–ZrO_2 samples, because they are stable against deactivation by sublimation, decomposition, and sintering and thus retain high isomerization selectivities (71% at 523 K and 36% conversion) and rates [9].

n-Heptane isomerization kinetic and isotopic tracer data on Pt/WO_x–ZrO_2 and Pt/SO_x–ZrO_2 are consistent with isomerization reactions that proceed via chain reactions involving hydrogen transfer from alkanes, H_2, or hydride donors, such as adamantane, to adsorbed isomerized heptanes [9,48]. This mechanism contrasts that discussed previously for n-heptane isomerization on oxygen-modified WC and Pt/WO_x–Al_2O_3 catalysts, in which alkene intermediates form on the dehydrogenation function, diffuse to and isomerize on the WO_x acid-function. At the higher temperature (623 K vs. 473 K) required for significant iso-

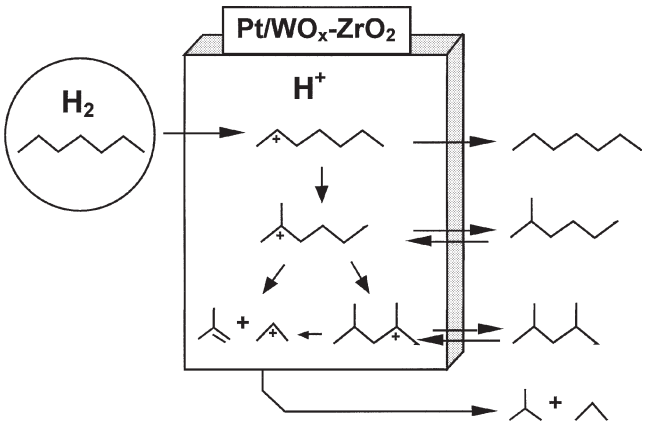

Scheme 1.

Table 6
n-Heptane isomerization selectivity, reaction kinetics, and isotopic tracer data on Pt/WO_x–ZrO_2 [0.3 wt.% Pt, 12.7 wt.% W, Pt/WO_x–ZrO_2 oxidation at 723 K after WO_x–ZrO_2 oxidation at 1073 K].

Isomerization selectivity (%)[a]	89
n-Heptane reaction order[b]	0.9
H_2 reaction order[b]	−0.5–0
Adamantane reaction order[a,c]	0.05
Deuterium content in n-heptane (%)[d]	82
Deuterium content in methylhexanes (%)[d]	83

[a] [473 K, 650 kPa H_2, 100 kPa n-heptane, 50% n-heptane conversion]. [b] [473 K, 800–2900 kPa H_2, 33–200 kPa n-heptane]. [c] [0–1.0 mol.% adamantane]. [d] [343 K, 3.7 kPa n-heptane, 97 kPa D_2, 5% n-heptane conversion].

merization rates on WC and WO_x–Al_2O_3 catalysts, equilibrium alkene concentrations are much higher and provide an effective diffusive pathway for communication between the two types of sites required in bifunctional isomerization pathways. On Pt/WO_x–ZrO_2 and Pt/SO_x–ZrO_2 (at 473 K), alkenes are not detected in the gas phase and hydrogen transfer reactions via surface diffusion of hydrogen provide an alternate and more effective pathway for communication between hydrogenation sites and acid sites.

On Pt/WO_x–ZrO_2, n-heptane adsorption-desorption steps are quasi-equilibrated and surface isomerization steps limit the overall rate (scheme 1). As a result, facile hydrogen transfer steps decrease the surface residence time of intermediates and lead to desorption of isomers before undesired β-scission events occur on the acid sites. Isomerization turnover rates are first order in n-heptane and zero to negative order in H_2 (table 6), suggesting that surface isomerization is rate-limiting and that hydrogen transfer steps decrease the coverage of surface intermediates. Hydrogen transfer occurs primarily using hydrogen adatoms formed by H_2 dissociation on surface Pt atoms, which spillover onto WO_x centers (scheme 2). These hydrogen transfer steps are inhibited on Pt/SO_x–ZrO_2 catalysts by the difficult dissociation of H_2 on Pt clusters poisoned by sulfur species, which leads to high cracking selectivity.

Addition of hydrogen transfer co-catalysts, such as adamantane, increase n-heptane isomerization rate and selectivity on Pt/SO_x–ZrO_2, but not on Pt/WO_x–ZrO_2, because hydrogen transfer steps are quasi-equilibrated on the latter and do not benefit from co-catalysts that increase the rate of these reactions [9]. Mixtures of n-C_7H_{16}–D_2 quickly reach H–D equilibrium and lead to complete scrambling and binomial deuterium distribution in "unreacted" n-heptane and in all reaction products, confirming the reversible (quasi-equilibrated) nature of n-heptane adsorption-desorption steps on Pt/WO_x–ZrO_2 [9].

Near-edge X-ray absorption studies and temperature-programmed reduction studies have detected the reduction of W^{6+} centers during hydrogen treatment at 473–673 K [9,12]. Site titration studies using H_2, O_2, and CO show that hydrogen uptake exceeds monolayer coverages on surface Pt atoms and that O_2 uptake is significantly higher than that of H_2 (table 7), suggesting that hydrogen adatoms spillover onto reduced WO_x centers during H_2 treatments at typical isomerization reaction temperatures. At higher reduction temperatures, H_2 uptakes markedly decrease and O_2 uptakes increase; these effects appear to be related to decoration of Pt crystallites by oxygen-deficient WO_x, as also proposed to explain similar effects in TiO_2 supported metal particles [49]. The spillover of hydrogen adatoms appears to involve the formation of acidic hydrogens on the WO_x clusters (scheme 3). Hydrogen adatoms formed by homolytic dissociation of H_2 on Pt sites lose electron density to Lewis acid WO_x clusters, which delocalize the reduced charge and stabilize the protons. Thus, hydrogen adatoms become involved not only in the desorption of adsorbed intermediates, but also in the generation and maintenance of Brønsted acid sites. The formation of Brønsted acid sites during H_2 treatment has been directly observed by infrared measurements of pyridine adsorption on Pt/SO_x–ZrO_2 by Ebitani et al. [50]. They report that the density of Brønsted acid sites increases during contact with H_2 at temperatures typical of those required for their catalytic action. The density of Lewis acid sites concurrently de-

Table 7
Irreversible chemisorption uptake[a] of H_2, O_2, and CO on Pt/WO_x–ZrO_2 (0.3 wt.% Pt, 10 wt.% W).

Reduction temperature (K)	H/Pt	O/Pt	CO/Pt
473	0.63	1.25	0.30
673	0.092	2.04	0.050

[a] Room temperature adsorption; irreversibly chemisorbed species are defined as those that cannot be removed by evacuation at room temperature.

$$(C_7H_{15})(W^{6+})_{n-1}(W^{5+})O_{3n} + H\text{–}Pt_x \longrightarrow (W^{6+}O_3)_n + C_7H_{16}(g) + Pt_x$$

Scheme 2.

$$H\text{–}H + (W^{6+}O_3)_n \rightleftarrows (H^+)_2(W^{6+})_{n-2}(W^{5+})_2O_{3n}$$

Scheme 3.

Table 8
Influence of the preparative method on the structure, activity, and acidity of WO_x–ZrO_2 catalysts oxidized at 1098 K [51].

	Impregnation[a]	Reflux-impregnation[b]	Co-precipitation[c]
W-loading (wt.% W)	15.0	16.9	15.5
Surface area (m^2/g)	32	62	62
% tetragonal ZrO_2	30	10	1
Bulk WO_3 present?	yes	yes	no
[d]Number of strong Brønsted acid sites (meq H^+/g)	0.002	0.002	0.004
[e]Pentane isomerization acid site turnover frequency (s^{-1})		2.8	3.9

[a] Prepared by metatungstate impregnation on pH 9 precipitated $ZrO_x(OH)_{4-2x}$. [b] Prepared by refluxing $ZrO_x(OH)_{4-2x}$ overnight prior to metatungstate impregnation. [c] Prepared by coprecipitation of metatungstate and $ZrOCl_2$ solutions at pH 9. [d] 2,6-dimethylpyridine adsorption results. [e] [483 K, 2 H_2/nC_5 mol ratio, LHSV = 2 cm^3 nC_5/ml-cat·h, 2400 kPa.]

creased, suggesting that Lewis acid sites are converted to Brønsted acid sites by contact with H_2. As a result, only techniques that measure the Brønsted acid site density under catalytic conditions provide an accurate value of the Brønsted acid site density available for reaction.

Several recent patents describe the synthesis and catalytic activity of WO_x–ZrO_2 and Pt/WO_x–ZrO_2 catalysts for cyclohexane ring-opening and isomerization, benzene hydrogenation, alkene oligomerization, aromatic alkylation with C_6^+ alkenes, toluene alkylation with methanol, aromatic trans-alkylation reactions, selective catalytic reduction of nitrogen oxides, and the hydrodesulfurization and hydrodenitrogenation of crude oils [11]. These authors report that maximum activity for pentane isomerization was found on WO_x–ZrO_2 samples (16 wt.% W, 1098 K oxidation) prepared by co-precipitation of $ZrOCl_2$ and ammonium metatungstate solutions, as opposed to impregnation of ammonium metatungstate on $ZrO_x(OH)_{4-2x}$ [51]. It appears that a better dispersion of metatungstate ions on amorphous $ZrO_x(OH)_{4-2x}$ is achieved during co-precipitation leading to higher surface area, lower monoclinic ZrO_2 content, and fewer inaccessible WO_x species within WO_3 clusters in the oxidized materials (table 8).

Santiesteban and coworkers also report that their most active WO_x–ZrO_2 catalyst contains few Brønsted acid sites (4 μmol H^+/g-cat) based on the amount of 2,6-dimethylpyridine needed to prevent n-pentane isomerization reactions [51]. They conclude that these minority Brønsted acid sites are 10^4 times more active in pentane isomerization reactions than Brønsted acid sites present in β-zeolite. The mechanism for n-pentane activation on these catalysts involves a C–H bond activation-initiation step leading to olefins, which can be used in carbocation chain reactions. It appears that a small amount of 2,6-dimethylpyridine titrates the strongest acid sites that are required to activate pentane and initiate these chain processes. 2,6-dimethylpyridine may titrate, however, both Lewis and Brønsted acid sites at the temperature they used to disperse this basic molecule (573 K). Thus, a greater number of acid sites may exist that can catalyze methyl-shift reactions, but only a few of those active sites may be involved in the C–H bond activation-initiation step. In addition, the density of Brønsted acid sites before (or after) catalytic reaction is much lower than those present during catalytic reactions of hydrocarbons. As a result, the density of Brønsted acid sites measured by amine adsorption will underestimate the density present at reaction conditions, because Brønsted acid sites cannot survive in the absence of H_2 or hydrocarbon reactants.

Recent studies of the thermal desorption of alcohols show that acid sites on WO_x–ZrO_2 catalysts have similar acid strength as H-mordenite [52]. Infrared measurements of adsorbed pyridine show that WO_x–ZrO_2 samples retain pyridine on their surface to higher temperatures than on WO_x–Al_2O_3, ZrO_2, or Al_2O_3 samples [53]. This pyridine adsorption study also shows qualitatively that WO_x–ZrO_2 samples that contain Pt have a higher density of Brønsted acid sites than those without Pt in an inert diluent [10].

On Pt/WO_x–ZrO_2, butane isomerization rates (573 K) are inhibited by H_2 (-0.7 reaction order) and are proportional to butane concentration (1.0 reaction order). Butane isomerization selectivity is decreased by the competitive metal-catalyzed hydrogenolysis of butane, which is promoted by H_2 (table 9) [10]. Hydrogenolysis does not occur on WO_x–ZrO_2 samples without Pt, but these samples are less active and deactivate more rapidly, apparently by carbon deposition [54]. ^{13}C isotopic tracer experiments during butane isomerization reactions on Pt/WO_x–ZrO_2 show that after initiation by a slow dehydrogenation step, bimolecular reactions lead to C_8 intermediates, which then undergo β-scission to form isomer products [55]. This mechanism is similar to that proposed earlier for butane isomerization on SO_x–ZrO_2 catalysts [56,57]. Addition of n-propylamine (98 μmol amine/g-cat) completely suppresses butane isomerization activity, but does not influence hydrogenolysis reactions requiring Pt sites [54], suggesting that the number of acid sites able to activate butane at 573 K on Pt/WO_x–

Table 9
Effect of platinum on the isomerization of n-butane on WO_x–ZrO_2 catalysts [10].

	[a]Pt/WO_x–ZrO_2 (acac)	[b]Pt/WO_x–ZrO_2 (std)	WO_x–ZrO_2
W-loading (wt.% W)	12	12	12
Pt-Loading (wt.% Pt)	1.2	1.2	0
Surface area (m^2/g)	44	45	36
CO/Pt adsorption	0.31	0.30	
[c]Butane isomerization rate (μmol/g-cat.s)	0.66	0.25	0.024
Butane hydrogenolysis rate (μmol/g-cat.s)	0.26	0	0
H_2 kinetic order	−0.8	−0.6	
n-C_4 kinetic order	0.9	1.0	
% coke at 1.5 h	0.013	0.066	0.072

[a] Pt impregnation with platinum acetylacetonate after high temperature oxidation of WO_x–ZrO_2 (1096 K). [b] Pt impregnation with $PtCl_6$ prior to high temperature oxidation of WO_x–ZrO_2 (1096 K). [c] [573 K, 67.5 kPa H_2, 33.8 kPa n-C_4, 2.4% maximum conversion].

ZrO_2 in the presence of H_2 may larger than the number able to activate pentane at 483 K on WO_x–ZrO_2 (4 μmol/g-cat).

8. Summary

Solid acid catalysts based on supported WO_x clusters are active and stable for isomerization, dehydration, and cracking reactions. Brønsted acid sites form on WO_x clusters when a lower valent element replaces W^{6+} or when W^{6+} centers reduce slightly during catalytic reactions. WO_x clusters of intermediate size provide the balance between reducibility and accessibility required to maximize the number of surface H^+ species in WO_x–ZrO_2, zirconium tungstate, and oxygen-modified WC catalysts. In WO_x–ZrO_2 and zirconium tungstate catalysts, these WO_x clusters of intermediate size form after oxidative treatments that sinter ZrO_2 crystallites and increase WO_x surface density. In oxygen-modified WC catalysts, these WO_x clusters form after oxygen chemisorption of high surface area WC powders. Distorted octahedral WO_x clusters of intermediate size on ZrO_2 were detected by X-ray absorption and UV-visible spectroscopies and differ markedly in electronic structure, reduction behavior, and isomerization rate and selectivity from tungstate groups supported on Al_2O_3 and from bulk WO_3 catalysts.

The unique acid properties on WO_x–ZrO_2 catalysts appear to be related to their ability to form $W^{6-n}O_3$(n-H^+) centers under reducing conditions at low temperatures. These centers can stabilize carbocationic reactive intermediates by delocalizing the corresponding negative charge among several oxygen atoms. This delocalization of charge in supported WO_x clusters is similar to the permanent delocalization of negative charge throughout the $(WO_3)_{12}$ shell in 12-tungstophosphoric acid. Hydrogen is involved in the generation and maintenance of Brønsted acid sites during catalytic reactions on WO_x clusters. As a result, Brønsted acid site density measurements must be carried out under reaction conditions, because the density of these sites during catalysis can differ significantly from those before or after reaction.

Hydrogen transfer reactions play a critical role in alkane isomerization elementary steps and benefit from the presence of H_2 dissociation sites and Brønsted acid sites during hydroisomerization reactions. The addition of a metal function to supported WO_x acid catalysts leads to active and stable alkane hydroisomerization catalysts. Bifunctional n-heptane isomerization reactions at 623 K on oxygen-modified WC and Pt/WO_x–Al_2O_3 catalysts proceed via alkene intermediates that provide effective diffusive pathways for the kinetic coupling of steps occurring on dehydrogenation and acid sites. n-Heptane isomerization reactions at lower temperatures require alternative pathways for coupling these dehydrogenation and acid sites, because low equilibrium alkene concentrations minimize the role of bifunctional pathways involving gas phase alkenes. Hydrogen transfer reactions on Pt/WO_x–ZrO_2 catalysts provide an alternate and more effective pathway for communication between dehydrogenation and acid sites and lead to high alkane hydroisomerization rates and selectivities. Quasi-equilibrated hydrogen transfer steps decrease the surface residence time of intermediates and lead to desorption of isomers before undesired β-scission events occur on acid sites. In addition, hydrogen dissociation at low temperatures leads to higher Brønsted acid site densities by migration of hydrogen adatoms from Pt to WO_x clusters.

Acknowledgement

The authors would like to acknowledge financial support for this work from the National Science Foundation (CTS-9510575). We would also like to thank Prof. Gustavo Fuentes (UAM-Iztapalapa, Mexico) and Dr. George Meitzner (Edge Analytical) for helpful insights, technical discussions, and research collaborations related to the UV-visible and X-ray absorption spectroscopic studies described in this review article. X-ray absorption experiments were performed at Stanford Synchrotron Radiation Laboratory (SSRL) supported, in part, by US Department of Energy.

References

[1] M. Misono and T. Okuhara, Chemtech 23 (11) (1993) 23.
[2] J.M. Thomas, Scientific American 266 (4) (1992) 112.
[3] R. Srinivasan, R.A. Keogh, D.R. Milburn and B.H. Davis, J. Catal. 153 (1995) 123.
[4] M. Hino and K. Arata, J. C. S. Chem. Commun. (1987) 1259.
[5] D. Farcasiu, A. Ghenciu and G.J. Miller, J. Catal. 134 (1992) 118.
[6] S.L. Soled, N. Dispenziere and R. Saleh, Stud. Surf. Sci. Catal. 73 (1992) 77.
[7] Exxon Research and Engineering Company (1995), US Patent # 5,422,327.
[8] S.L. Soled, S. Miseo, J.E. Baumgartner, W.E. Gates, D.G. Barton and E. Iglesia, in: *Proc. 13th Int. Conf. Catal.* (The Taniguchi Foundation, Kobe, Japan, 1994) p. 17.

[9] E. Iglesia, D.G. Barton, S.L. Soled, S. Miseo, J.E. Baumgartner, W.E. Gates, G.A. Fuentes and G.D. Meitzner, Stud. Surf. Sci. Catal. 101 (1996) 533.
[10] G. Larsen, E. Lotero, S. Raghavan, R.D. Parra and C.A. Querini, Appl. Catal. A 139 (1996) 201.
[11] Mobil Oil Corp., US Patent # 5,345,026 (1994); 5,382,731 (1995); 5,401,478 (1995); 5,449,847 (1995); 5,453,556 (1995); 5,510,309 (1996); 5,516,954 (1996); 5,543,036 (1996); 5,552,128 (1996); 5,563,310 (1996); 5,563,311 (1996); 5,608,133 (1997).
[12] D.G. Barton, S.L. Soled, G.M. Meitzner and E. Iglesia, submitted to J. Catal. (1997).
[13] J.B. Moffat, Stud. Surf. Sci. Catal. 20 (1985) 157.
[14] M. Misono, Catal. Rev. Sci. Eng. 29 (1987) 269.
[15] C.H. Kline and V. Kollonitsch, Ind. Eng. Chem. 57 (1965) 53.
[16] P. Sabatier, in: *Catalysis in Organic Chemistry* (Van Nostrand, New York, 1923).
[17] J.E. Benson, H.W. Kohn and M. Boudart, J. Catal. 5 (1966) 307.
[18] T. Yamaguchi, Y. Tanaka and K. Tanabe, J. Catal. 65 (1980) 442.
[19] R.H. Bliss and B.F. Dodge, Ind. Eng. Chem. 29 (1937) 19.
[20] P. Tittarelli, A. Iannibello and P.L. Villa, J. Solid State Chem. 37 (1981) 95.
[21] S.L. Soled, L.L. Murrell, I.E. Wachs, G.B. McVicker, L.G. Sherman, S.S. Chan, N.C. Dispenziere and R.T.K. Baker, in: *ACS Symposium Series* (American Chemical Society, Washington DC, 1985) p. 165.
[22] M.A. Vuurman and I.E. Wachs, J. Phys. Chem. 96 (1992) 5008.
[23] J.A. Horsley, I.E. Wachs, J.M. Brown, G.H. Via and F.D. Hardcastle, J. Phys. Chem. 91 (1987) 4014.
[24] S.L. Soled, G.B. McVicker, L.L. Murrell, L.G. Sherman, N.C. Dispenziere, S.L. Hsu and D. Waldman, J. Catal. 111 (1988) 286.
[25] L.L. Murrell, D.C. Grenoble, C.J. Kim and N.C. Dispenziere, J. Catal. 107 (1987) 463.
[26] E. Iglesia, J.E. Baumgartner, F.H. Ribeiro and M. Boudart, J. Catal. 131 (1991) 523.
[27] M. Misono, Mat. Chem. Phys. 17 (1987) 103.
[28] T. Okuhara, T. Nishimura, H. Watanabe and M. Misono, J. Mol. Catal. 74 (1992) 247.
[29] S. Soled, S. Miseo, G. McVicker, W.E. Gates, A. Gutierrez and J. Paes, Catal. Today 36 (1997) 441.
[30] K. Takahashi, T. Okuhara and M. Misono, Chem. Lett. 6 (1985) 8418.
[31] K. Nowinska, R. Fiedorow and J. Adamiec, J. Chem. Soc. Faraday Trans. 87 (1991) 749.
[32] M.A. Schwegler, P. Vinke, M. van der Eijk and H. van Bekkum, Appl. Catal. A 80 (1992) 41.
[33] T. Baba and Y. Ono, Appl. Catal. 22 (1986) 321.
[34] F.H. Ribeiro, M. Boudart, R.A. Dalla-Betta and E. Iglesia, J. Catal. 130 (1991) 498.
[35] R.B. Levy and M. Boudart, Science 181 (1973) 547.
[36] A. Katrib, V. Logie, N. Saurel, P. Wehrer, L. Hilaire and G. Maire, Surf. Sci. 377 (1997) 754.
[37] E. Iglesia, F.H. Ribeiro, M. Boudart and J.E. Baumgartner, Cat. Today 15 (1992) 307.
[38] Y.P. Zhuang and A. Frennet, J. Catal. 163 (1996) 223.
[39] Y. Izumi, Catal. Today 33 (1997) 371.
[40] H. Momose, K. Kusumoto, Y. Izumi and Y. Mizutani, J. Catal. 77 (1982) 23.
[41] R.C. Garvie and M.F. Goss, J. Mater. Sci. 21 (1986) 1253.
[42] S. Morin, N.S. Gnep and M. Guisnet, J. Catal. 159 (1996) 296.
[43] R.S. Weber, J. Catal. 151 (1995) 470.
[44] M.A. Butler, J. Appl. Phys. (1977) 1916.
[45] E. Shadle, B. Hedman, K.O. Hodgson and E.I. Solomon, Inorg. Chem. 33 (1994) 4235.
[46] I.E. Wachs, *Characterization of Catalytic Materials* (Butterworth-Heinnemann, Boston, 1992).
[47] M.T. Pope, *Heteropoly and Isopoly Oxometallates* (Springer, Berlin, 1983).
[48] E. Iglesia, S.L. Soled and G.M. Kramer, J. Catal. 144 (1993) 238.
[49] S.J. Tauster, S.C. Fung and R.L. Garten, J. Amer. Chem. Soc. 100 (1978) 170.
[50] K. Ebitani, J. Tsuji, H. Hattori and K. Kita, J. Catal. 135 (1992) 609.
[51] J.G. Santiesteban, J.C. Vartuli, S. Han, R.D. Bastian and C.D. Chang, J. Catal. 168 (1997) 431.
[52] G. Larsen, E. Lotero, L.M. Petkovic and D.S. Shobe, J. Catal. 169 (1997) 67.
[53] G. Larsen, S. Raghavan, M. Marquez and E. Lotero, Catal. Letters. 37 (1996) 57.
[54] G. Larsen and L.M. Petkovic, Appl. Catal. A 148 (1996) 155.
[55] G. Larsen and L.M. Petkovic, J. Molec. Catal. A 113 (1996) 517.
[56] F. Garin, L. Seyfried, P. Girard, G. Maire, A. Abdulsamad and J. Sommer, J. Catal. 151 (1995) 26.
[57] V. Adeeva, G.D. Lei and W.M.H. Sachtler, Appl. Catal. A 118 (1994) L11.